

Partial and complete qubit estimation using a single observable: optimization and quantum simulation

Cristian A. Galvis Florez, J. Martínez-Cifuentes, K. M. Fonseca-Romero*

*Departamento de Física, Universidad Nacional de Colombia - Sede Bogotá, Facultad de Ciencias, Grupo de Óptica e Información Cuántica, Carrera 30 Calle 45-03, C.P. 111321, Bogotá, Colombia

E-mail: cagalvisf@unal.edu.co, ajmartinezc@unal.edu.co, kmfonsecar@unal.edu.co

27 January 2023

Abstract. Quantum state estimation is an important task of many quantum information protocols. We consider two families of unitary evolution operators, one with a one-parameter and the other with a two-parameter, which enable the estimation of a single spin component and all spin components, respectively, of a two-level quantum system. To evaluate the tomographic performance, we use the quantum tomographic transfer function (qTTF), which is calculated as the average over all pure states of the trace of the inverse of the Fisher information matrix. Our goal is to optimize the qTTF for both estimation models. We find that the minimum qTTF for the one-parameter model is achieved when the entangling power of the corresponding unitary operator is at its maximum. The models were implemented on an IBM quantum processing unit, and while the estimation of a single-spin component was successful, the whole spin estimation displayed relatively large errors due to the depth of the associated circuit. To address this issue, we propose a new scalable circuit design that improves qubit state tomography when run on an IBM quantum processing unit.

Keywords: Quantum state estimation, Quantum tomographic transfer function, Quantum Computing, IBM Quantum Experience.

1. Introduction

The concept of quantum mechanical computers was first proposed in the works of Feynman [1, 2]. Soon, several quantum algorithms were developed that are more efficient than their classical counterparts [3, 4]. These algorithms have been implemented in current quantum computers [5, 6] using a few qubits. One of the key tasks in assessing the performance of these quantum algorithms is the estimation of the computer's quantum state [7, 8]. This is particularly important in quantum cryptography, where

the qubit state needs to be accurately specified both at the source and after transmission [9]. Due to errors in state preparation and processing, it is essential to have accurate state estimates at various stages of quantum protocols. Various methods for state estimation [10] have been implemented, such as maximal entropy [11, 12], maximum likelihood [13], Bayesian methods [14], and linear regression estimation [15]. These methods may vary in their resource requirements, such as the number of measurements needed or the knowledge of the system's evolution. For example, usual tomography assume access to n^2 different measurements; adaptive methods, the possibility to measure arbitrary observables; stroboscopic methods [16, 17, 18] require the knowledge of the evolution of the system. Like the single-observable state estimation [19], stroboscopic tomography requires only a single observable. However, single-observable tomography also requires an auxiliary system of dimension at least equal to that of the system whose state is estimated and the joint evolution at a single instant of time.

Peres' model [20], a particular instance of the von Neumann model of measurement, involves an auxiliary two-level system to measure a qubit observable (sec. 2.1). Its extension [21], which employs two auxiliary two-level systems (sec. 2.2), is an example of a variant of the single-observable tomographic method, in which the system is not directly measured. This would be the case of cavity QED, for example, where two-level atoms are used as probes to measure the state of the confined photons.

Peres' model and its extension are parameterized by one or two parameters, respectively. Here, we consider and solve the problem of finding the parameters which optimize the tomographic performance of these models, as measured by the quantum tomographic transfer function (qTTF) [22]. The qTTF is the average, over all pure states of the system, of the trace of the inverse of the Fisher information matrix. The models considered in this work, are run on a five-qubit IBM quantum processing unit (QPU). The experimental qTTF is found by averaging the error over a set of six points, equally spaced on the Bloch sphere. This experimental quantifier is satisfactory for Peres' model and for an alternative model of qubit state estimation, but it is large for the circuit implementation of the extended Peres' model (sec. 3). The alternative model, which employs only two CNOT gates, is proposed, optimized and run on an IBM QPU (subsection 3.3). An alternative proposal for multiqubit states, implemented on IBM quantum processors, use entangled bases [23]. Scalability of our model is discussed in the last section of this paper (section 4).

2. Partial and complete spin estimation methods

2.1. Estimation of a single spin component

The spin component s_z of a qubit S can be estimated by using an auxiliary qubit (meter) A . The interaction between the system and meter is described by the Hamiltonian $H_A = g |1^S\rangle \langle 1^S| \otimes |1^A\rangle \langle 1^A|$ [20], where g is a coupling constant. The associated evolution

operator is

$$U_A(\theta) = e^{-iH_A T/\hbar} = \begin{pmatrix} 1 & 0 & 0 & 0 \\ 0 & 1 & 0 & 0 \\ 0 & 0 & 1 & 0 \\ 0 & 0 & 0 & e^{-i\theta} \end{pmatrix}. \quad (1)$$

$U(\theta)$, which has been written in two-qubit basis in the lexicographic order $|00\rangle, |01\rangle, |10\rangle, |11\rangle$, has the form of a *controlled phase gate* ($C_P(\theta)$). The evolution operator depends on the single parameter $\theta = gT/\hbar$, where T represents the interaction time. Due to the periodicity of $U_A(\theta)$, we consider $\theta \in [0, 2\pi)$. The initial state of the qubit-meter system is assumed to be $|\psi_0^S\rangle \otimes |+\rangle$, where the initial states of system and meter are, respectively, $|\psi_0^S\rangle = c_0|0\rangle + c_1|1\rangle$, and $|+\rangle = \frac{1}{\sqrt{2}}(|0\rangle + |1\rangle)$. Coefficients c_0 and c_1 satisfy the normalization condition $|c_0|^2 + |c_1|^2 = 1$. At time T , the meter is measured in the σ_x basis. It is detected in the state $|+\rangle$ ($\sigma_x|+\rangle = |+\rangle$) with probability $P_+ = P_0$ or in the state $|-\rangle$ ($\sigma_x|-\rangle = -|-\rangle$) with probability $P_- = P_1$. Here,

$$P_0 = |c_0|^2 + |c_1|^2 \cos^2 \frac{\theta}{2} = \frac{1}{2} \left(1 + \cos^2 \frac{\theta}{2} \right) + \frac{1}{2} \sin^2 \frac{\theta}{2} s_z, \quad (2)$$

$$P_1 = |c_1|^2 \sin^2 \frac{\theta}{2} = \frac{1}{2} \sin^2 \frac{\theta}{2} (1 - s_z), \quad (3)$$

and $s_z = \langle \psi_0^S | \sigma_z^S | \psi_0^S \rangle = |c_0|^2 - |c_1|^2$. In terms of the probabilities of detection, the parameter s_z can be estimated using the relation

$$s_z = \csc^2 \left(\frac{\theta}{2} \right) \left(P_0 - P_1 - \cos^2 \left(\frac{\theta}{2} \right) \right). \quad (4)$$

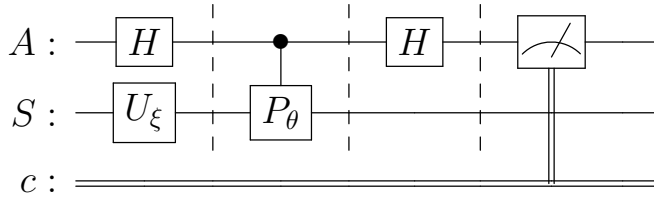


Figure 1. Quantum circuit for the estimation of a single spin component of a qubit S using the auxiliary qubit A .

The circuit that represents this process, shown in Figure 1, is divided into four sections: preparation, interaction, change of basis, and measurement. Taking into account that the qubits' default state in quantum circuits is $|0\rangle$, the initial state of the qubit-meter system is $U_\xi |0^S\rangle \otimes U_H |0^A\rangle$, where U_ξ denotes a general single-qubit gate rotation defined by a set of angles ξ such that $U_\xi |0^S\rangle = |\psi_0^S\rangle$, and U_H a Hadamard gate.

The evolution operator (1), is implemented by a $C_P(\theta)$ gate. Since only measurements on the σ_z basis are available, it is necessary to perform a change of

basis (the Hadamard gate of the third section) to measure the auxiliary qubit in the σ_x basis.

It is essential to find an estimation for s_z , and to characterize the associated error (the square root of the variance). Any unbiased estimator satisfies the Cramér-Rao bound $\text{Cov}(\mathbf{s}, \mathbf{s}) \geq \mathbb{F}^{-1}(\mathbf{s})$, where \mathbf{s} is the vector of parameters to be estimated, $\text{Cov}(\mathbf{s}, \mathbf{s})$ the corresponding covariance matrix, and $\mathbb{F}(\mathbf{s})$ the associated Fisher information matrix. The elements of the Fisher matrix are given by [24]

$$F_{\mu\nu}(\mathbf{s}) = -\mathbb{E} \left(\frac{\partial^2 \ln P(\mathbf{s})}{\partial s_\mu \partial s_\nu} \right),$$

where \mathbb{E} denotes the statistical expectation value. We consider that the multinomial distribution $P(\mathbf{n}|\mathbf{s}) = (\sum_k n_k)! \prod_k p_k^{n_k} / (n_k!)$, gives the probability that n_k events corresponding to the k -th outcome were detected. Assuming the probabilities p_k to linearly depend on the parameters s_μ we get

$$F_{\mu\nu}(\mathbf{s}) = \mathbb{E} \left(\sum_k \frac{n_k}{p_k^2} \frac{\partial p_k}{\partial s_\mu} \frac{\partial p_k}{\partial s_\nu} \right).$$

Using $n_k = N p_k$, where $N = \sum_k n_k$, and taking into account that the resulting expression is not longer a function of n_k , we obtain

$$F_{\mu\nu}(\mathbf{s}) = N \sum_{j=0}^1 \frac{1}{p_j} \frac{\partial p_j}{\partial s_\mu} \frac{\partial p_j}{\partial s_\nu}. \quad (5)$$

The N factor, which describes a variance proportional to N^{-1} , will be ignored, unless we explicitly consider the effect of the sample size. Here, s_z is the only parameter to be estimated. Hence, the Fisher matrix becomes just a number, whose inverse is

$$F^{-1}(c_0, c_1, \theta) = \frac{4P_0(c_0, c_1)P_1(c_0, c_1)}{\sin^4 \frac{\theta}{2}}. \quad (6)$$

Since $F^{-1}(c_0, c_1, \theta)$ is the lower limit to the variance associated to s_z , it is defined as the estimation error. In Appendix A.1, we show that, in the limit $N \rightarrow \infty$, the variance of the average of s_z over N shots coincides with the Fisher error

$$\text{Var}(\hat{s}_z) \rightarrow \frac{1}{N-1} F^{-1} \rightarrow \frac{1}{N} F^{-1}. \quad (7)$$

To study the dependence of the error on the initial state of qubit S , we parameterize the state of the system using $\xi = \{\alpha_1, \alpha_2\}$ as $c_0 = e^{i\alpha_2} \cos \alpha_1$ and $c_1 = e^{-i\alpha_2} \sin \alpha_1$, where $\alpha_1 \in [0, \pi/2]$, and $\alpha_2 \in [0, \pi]$. The resulting expression for the error,

$$\tilde{F}^{-1}(\alpha_1, \alpha_2, \theta) = F^{-1}(c_0(\alpha_1, \alpha_2), c_1(\alpha_1, \alpha_2), \theta) = 4 \sin^2(\alpha_1) (\csc^2(\theta/2) - \sin^2(\alpha_1)),$$

is independent of α_2 . This error is plotted in Figure 2 for different values of θ in the interval $[\pi/2, \pi]$. Values of θ between 0 and $\frac{\pi}{2}$, not depicted in Figure 2, have larger

estimation errors. It can be seen that, for a given fixed initial state, $\theta = \pi$ produces the least error. Hence, for the interaction considered in this work, it is convenient to use $\theta = \pi$ to obtain the best estimation of s_z .

The maximum error, for fixed θ , satisfy

$$\frac{\partial F^{-1}}{\partial \alpha_1} = 4 \sin(2\alpha_1) (\csc^2(\theta/2) - 2 \sin^2 \alpha_1) = 0. \quad (8)$$

If $0 \leq \theta \leq \pi/2$ ($\pi/2 \leq \theta \leq \pi$) the maximum error occurs at $\alpha_1 = \pi/2$ ($\alpha_1 = \arcsin(\frac{1}{\sqrt{2}} \csc(\theta/2))$) where $F^{-1} = 4(\csc^2(\theta/2) - 1)$ ($F^{-1} = \csc^4(\theta/2)$). Hence, the maximum error for constant θ is $F_{max}^{-1} = \max(4(\csc^2(\theta/2) - 1), \csc^4(\theta/2))$.

Since the system-meter state is pure, its entanglement can be quantified by the entropy of either reduced density matrix, $\rho_S = \text{tr}_A(|\psi_{AS}\rangle\langle\psi_{AS}|)$, or $\rho_A = \text{tr}_S(|\psi_{AS}\rangle\langle\psi_{AS}|)$. Here $|\psi_{AS}\rangle = (1/\sqrt{2})(c_0|00\rangle + c_0|01\rangle + c_1|10\rangle + c_1e^{-i\theta}|11\rangle)$. The von Neumann entropy [25] of the system, after the interaction with the meter, is

$$E(\rho_S) = -\text{Tr}(\rho_S \log \rho_S) = -\lambda_+ \log \lambda_+ - \lambda_- \log \lambda_-, \quad (9)$$

where $\lambda_{\pm} = (1/2)(1 \pm \sqrt{x})$ and $x = 1 - \sin^2(2\alpha_1) \sin^2(\theta/2)$. System's entropy $E(\rho_S)$ is not only qualitatively similar to the error F^{-1} , it also vanishes for the same combinations of α_1 and θ : ($\alpha_1 = 0$, any θ), and ($\alpha_1 = \pi/2$, $\theta = \pi$). The initial state corresponding to $\alpha_1 = 0$, $|0^S\rangle|+^A\rangle$, is left unchanged by the evolution operator (1). On the other hand, the initial state when $\alpha_1 = \frac{\pi}{2}$ and $\theta = \pi$, $|1^S\rangle|+^A\rangle$, changes to $|1^S\rangle|-^A\rangle$. The error vanishes in both cases because only one outcome is available.

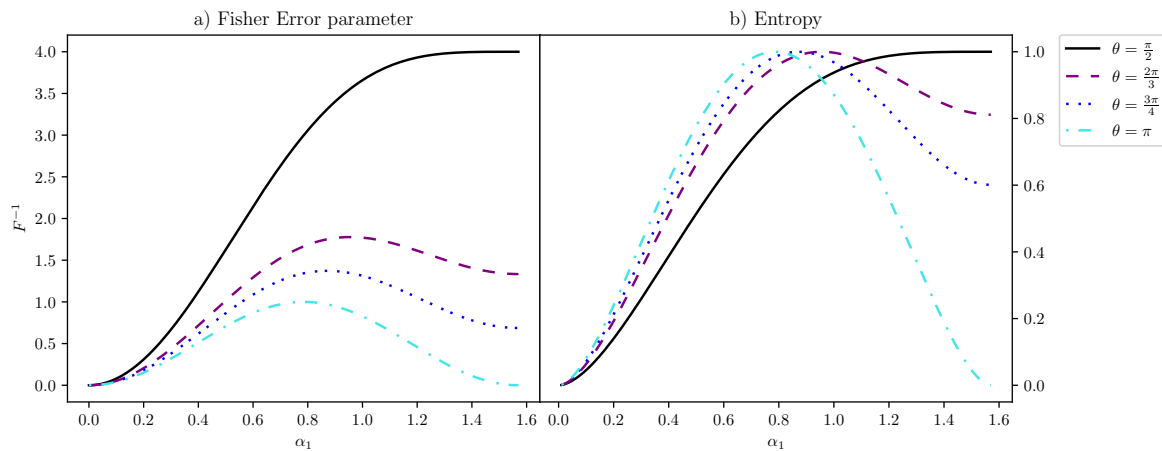


Figure 2. a) Error F^{-1} as a function of α_1 for $\theta = \frac{\pi}{2}, \frac{2\pi}{3}, \frac{3\pi}{4}$ and π . Error decreases as $\theta \rightarrow \pi$. b) Entropy of the system state, after the interaction, as a function of α_1 for $\theta = \frac{\pi}{2}, \frac{2\pi}{3}, \frac{3\pi}{4}$ and π . The entropy and the error vanish for the same values of α_1 and θ .

To study the dependence of the error of the estimation only on the coupling parameter θ , we define the average of $F^{-1}(\alpha_1, \alpha_2, \theta)$ (we have dropped the tilde to

lighten the notation) over the set of initial pure states of the system,

$$\overline{F^{-1}}(\theta) = \frac{1}{\pi} \int_0^{\pi/2} d\alpha_1 \int_0^\pi d\alpha_2 F^{-1}(\alpha_1, \alpha_2, \theta) \sin(2\alpha_1). \quad (10)$$

This average is equivalent to the natural generalization of the *quantum tomographic transfer function* (qTTF), first defined in [22], for the case where only one parameter is estimated. Optimization of the qTTF over θ allows us to determine which $U(\theta)$ performs better for the estimation of s_z . We obtain $\overline{F^{-1}}(\theta) = \frac{2}{3}(2 + \cos\theta) \csc^2(\theta/2)$, which is a monotonic decreasing function in $[0, \pi]$. $\overline{F^{-1}}(\theta)$ diverges for $\theta \rightarrow 0$ and attains its minimum at $\theta = \pi$, $\overline{F^{-1}}(\pi) = 2/3$.

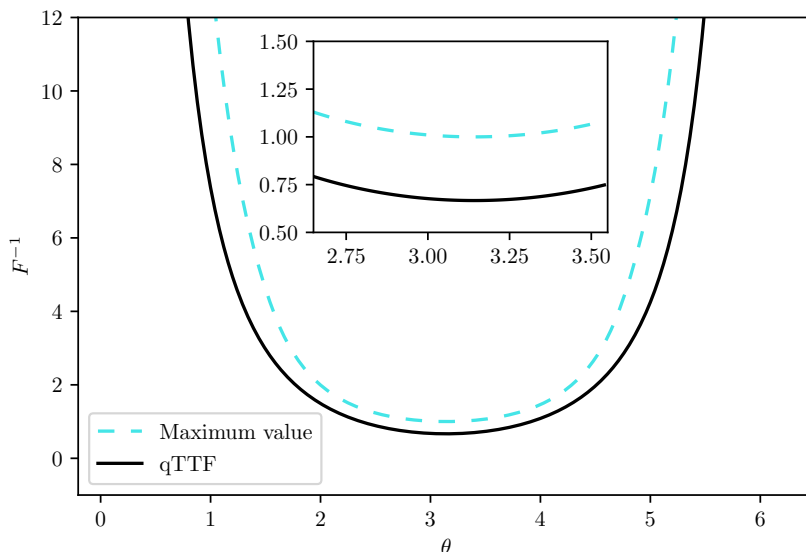


Figure 3. qTTF $\overline{F^{-1}}$ (solid line) and maximum error F_{max}^{-1} (dashed line) as functions of the coupling parameter θ .

Figure 3 shows $\overline{F^{-1}}(\theta)$ and the maximum error for fixed θ , F_{max}^{-1} , as a function of θ . As can be seen, the value $\theta = \pi$ corresponds to the coupling value with the minimum average error, which agrees with the results shown in Figure 2, where the configuration with $\theta = \pi$ has the lowest values of the error $F^{-1}(\alpha_1, \alpha_2, \theta)$. This value coincides with the maximum entangling power of the unitary evolution U [26].

2.2. Complete qubit state estimation

The complete initial state of qubit S can be estimated using two auxiliary meters A and B . We consider the interaction Hamiltonian

$$H_{AB} = (\lambda_A \Pi_1^S \otimes \Pi_1^A \otimes I^B + \lambda_B \Pi_+^S \otimes I^A \otimes \Pi_1^B), \quad (11)$$

where $\Pi_k^M = |k^M\rangle\langle k^M|$, with $k = 1, +$ and $M = A, B$. Here, I_A and I_B are the identity operators associated to the Hilbert spaces of meters A and B , respectively, and λ_A, λ_B

are constants. The eigenstates of σ_x are denoted by $|+\rangle$ and $|-\rangle$. The time evolution operator at time T , $U_{AB}(\theta_A, \theta_B)$,

$$U_{AB}(\theta_A, \theta_B) = e^{-iH_{AB}T/\hbar} = \exp(-i\theta_A \Pi_1^S \otimes \Pi_1^A \otimes I^B - i\theta_B \Pi_+^S \otimes I^A \otimes \Pi_1^B) \quad (12)$$

depends on the parameters $\theta_A = (\lambda_A T/\hbar)$ and $\theta_B = (\lambda_B T/\hbar)$.

As in the previous section, the A and B meters are prepared in the state $|+\rangle = (|0\rangle + |1\rangle)/\sqrt{2}$ and qubit S is prepared in an arbitrary state $|\psi_0^S\rangle = c_0|0\rangle + c_1|1\rangle$. The joint initial state $|\Psi(0)\rangle = |\psi_0^S\rangle \otimes |+\rangle^A \otimes |+\rangle^B$ is transformed by the interaction into the final state

$$|\Psi_f\rangle = U_{AB}(\theta_A, \theta_B) |\Psi(0)\rangle = \frac{1}{2} \sum_{ij=0,1} U_{ij} |\psi_0^S\rangle \otimes |i^A, j^B\rangle, \quad (13)$$

where $|i^A, j^B\rangle = |i^A\rangle \otimes |j^B\rangle$ and

$$U_{00} = I, \quad U_{01} = e^{-i\theta_B \Pi_+^S}, \quad (14)$$

$$U_{10} = e^{-i\theta_A \Pi_1^S}, \quad U_{11} = e^{-\theta_A \Pi_1^S - i\theta_B \Pi_+^S}. \quad (15)$$

The probability p_{kl} that meters A and B are detected in states $|k^A\rangle$ and $|l^A\rangle$, respectively, $k, l = \pm$, is

$$p_{kl} = \frac{1}{4} s_0 + \sum_{\mu=1}^3 (a_\mu k + b_\mu l + c_\mu kl) s_\mu. \quad (16)$$

Here, $s_0 = 1$ and s_μ , $\mu = 1, 2, 3$, are the components of the Bloch vector of the initial state of the system $\rho_0^S = |\psi_0\rangle \langle \psi_0|$, $s_\mu = \text{tr}(\rho_0^S \sigma_\mu)$. The matrix σ_0 is the identity matrix, and σ_i , with $i = 1, 2, 3$ are the Pauli matrices. The coefficients a_μ , b_μ , and c_μ are given by $a_\mu = \frac{1}{2} \text{Tr}[A\sigma_\mu]$, $b_\mu = \frac{1}{2} \text{Tr}[B\sigma_\mu]$ and $c_\mu = \frac{1}{2} \text{Tr}[C\sigma_\mu]$, where

$$A = \frac{1}{16} \sum_{ij} U_{ij}^\dagger U_{1-i,j}, \quad B = \frac{1}{16} \sum_{ij} U_{ij}^\dagger U_{i,1-j}, \quad C = \frac{1}{16} \sum_{ij} U_{ij}^\dagger U_{1-i,1-j}. \quad (17)$$

The explicit expressions for coefficients a_μ , b_μ , and c_μ can be found in the Appendix B. Although we have assumed that qubit S is prepared in a pure initial state, equation (16) holds for pure and mixed initial states ρ_0^S .

By defining the probability vector $\mathbf{P} = (p_{00}, p_{01}, p_{10}, p_{11})^T$, and the state vector $\mathbf{S} = (s_0, s_1, s_2, s_3)^T$, we can write equation (16) as $\mathbf{P} = \mathbb{T}\mathbf{S}$, where \mathbb{T} is an implicitly defined matrix. If this matrix is invertible, we can estimate vector \mathbf{S} , associated with the initial state of the system, as

$$\mathbf{S} = \mathbb{T}^{-1}\mathbf{P}. \quad (18)$$

This equation lets us estimate the vector \mathbf{S} using the probabilities (frequencies) measured in meters A and B .

The *linear inversion estimation*, which we have just described, sometimes predicts non-positive semidefinite states. The *discrete maximum-likelihood estimator* [27, 28],

which can also be expressed in terms of the matrix \mathbb{T} and the probabilities \mathbf{P} , always predicts physical states. This estimator is computed iteratively using the *RρR Algorithm* [29]. The $\rho^{(n+1)}$ estimation is computed from the the previous estimation, $\rho^{(n)}$, estimation

$$\rho^{(n+1)} = \mathcal{N} [R(\rho^{(n)}) \rho^{(n)} R(\rho^{(n)})], \quad (19)$$

where $\mathcal{N}[\cdot]$ denotes normalization to trace unity of the corresponding operator. Here,

$$R = \sum_{\mu=0}^3 r_{\mu} \sigma_{\mu} \quad \text{and} \quad r_{\mu}^{(n)} = \sum_{q=1}^4 \frac{P_q}{\check{P}_q^{(n)}} T_{q\mu}.$$

The components of the vector of experimental frequencies \mathbf{P} are denoted by P_q , and $\check{P}_q^{(n)} = \sum_{\mu=0}^3 T_{q\mu} s_{\mu}^{(n)}$, where $s_{\mu}^{(n)}$ are the components of $\mathbf{S}^{(n)}$, the Bloch components of $\rho^{(n)}$. The initial state, $\rho^{(0)} = \sigma_0/2$ is the maximally mixed state.

To simulate the quantum state estimation we propose the three-qubit circuit shown in Figure 4. One of the qubits corresponds to the system S , whose initial state is going to be estimated; the other two correspond to the A and B meters.

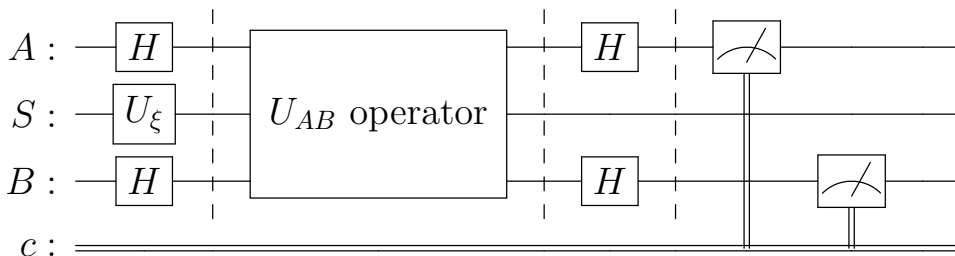


Figure 4. General structure of the quantum circuit used for the quantum state estimation.

The first part of the circuit corresponds to the initialization of the qubits, using a Hadamard gate for each of the meters, and a general U_{ξ} single-qubit gate rotation for the system. The second part is the core of the algorithm. The actual implementation of $U_{AB}(\theta_A, \theta_B)$ was found employing the transpilation algorithm of IBM-Q.

The Hadamard gates, at the end of the circuit, perform the transformation to the σ_x basis of the meters.

The Fisher information matrix for this model,

$$\mathbb{F} = \mathbb{D}^T (\mathbb{V} \mathbb{P}^{-1} \mathbb{V}^T) \mathbb{D}, \quad (20)$$

depends on the measurement matrix \mathbb{D} , and the auxiliary matrices \mathbb{V} and \mathbb{P}

$$\mathbb{D} = \begin{pmatrix} a_1 & b_1 & c_1 \\ a_2 & b_2 & c_2 \\ a_3 & b_3 & c_3 \end{pmatrix}, \quad \mathbb{V} = \begin{pmatrix} 1 & 1 & -1 & -1 \\ 1 & -1 & 1 & -1 \\ 1 & -1 & -1 & 1 \end{pmatrix}, \quad \mathbb{P} = \begin{pmatrix} p_{00} & 0 & 0 & 0 \\ 0 & p_{01} & 0 & 0 \\ 0 & 0 & p_{10} & 0 \\ 0 & 0 & 0 & p_{11} \end{pmatrix}.$$

To obtain this result, it is convenient to write the equation $\mathbf{P} = \mathbb{T}\mathbf{S}$ as $\mathbf{P} = (\frac{1}{4}\mathbf{1} + \mathbb{V}^T\mathbf{D}_0)s_0 + \mathbb{V}^T\mathbb{D}\mathbf{s}$, where $\mathbf{1} = (1, 1, 1, 1)^T$, $\mathbf{D}_0 = (a_0, b_0, c_0)^T$, and $\mathbf{s} = (s_1, s_2, s_3)^T$. Direct use of (5) gives $F_{\mu\nu} = \sum_{k=1}^4 \frac{1}{p_k} (\mathbb{V}^T\mathbb{D})_{k\mu} (\mathbb{V}^T\mathbb{D})_{k\nu}$, which can be written in matrix form as (20).

We define the error of the estimator as the trace of the inverse of the Fisher information matrix

$$\Delta(\alpha_1, \alpha_2, \theta_A, \theta_B) = \text{Tr}(\mathbb{F}^{-1}). \quad (21)$$

In the limit of large N , the variance of the estimator (\hat{s}^i) of the i -th component of the Bloch vector is related to an element of the Fisher error matrix

$$\text{Var}(\hat{s}^i) = \frac{1}{N} (\mathbb{F}^{-1})_{ii},$$

as shown in Appendix A.2.

The mean error over the whole set of initial pure states of the system, the qTTF, is used to characterize the error of the setup. It depends only on the parameters θ_A and θ_B . As mentioned in Section 2.1, an optimization of the average error over θ_A and θ_B allows the determination of which $U_{AB}(\theta_A, \theta_B)$ performs better for the estimation of the initial state of qubit S . Using the `scipy.optimize` package [30], we found that $\theta_A^{\min} \approx 3.45$ and $\theta_B^{\min} \approx -8.42$ minimize the mean error, which takes the value $\bar{\Delta}(\theta_A, \theta_B) \approx 17.0$.

The error $\Delta(\alpha_1, \alpha_2, \theta_A^{\min}, \theta_B^{\min})$, shown in Figure (5), displays moderate fluctuations as a function of the initial state.

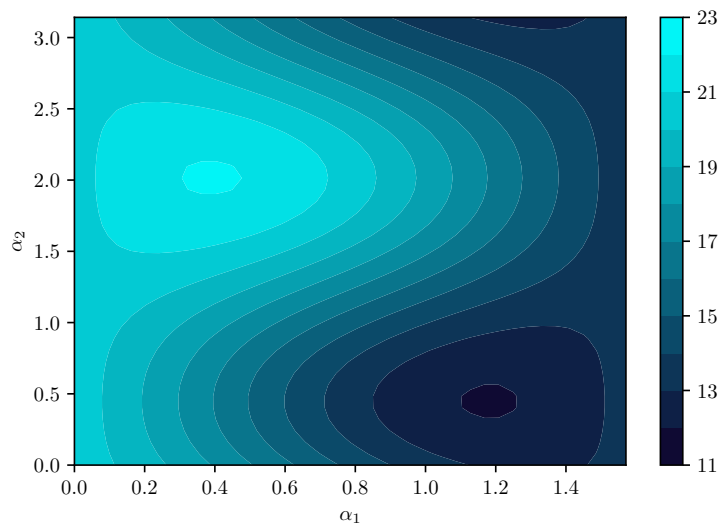


Figure 5. Fisher error, $\Delta(\alpha_1, \alpha_2, \theta_A^{\min} \approx 3.45, \theta_B^{\min} \approx -8.42)$ as a function of the initial state (parameterized by α_1 and α_2).

3. Results and Discussion

3.1. Estimation of a single spin component

We first simulate the estimation of s_z with the circuit in Figure 1. The results of the simulation for different values of θ with $c_0 = \frac{1}{2}$ and $c_1 = \frac{\sqrt{3}}{2}$ are shown in Figure 6.

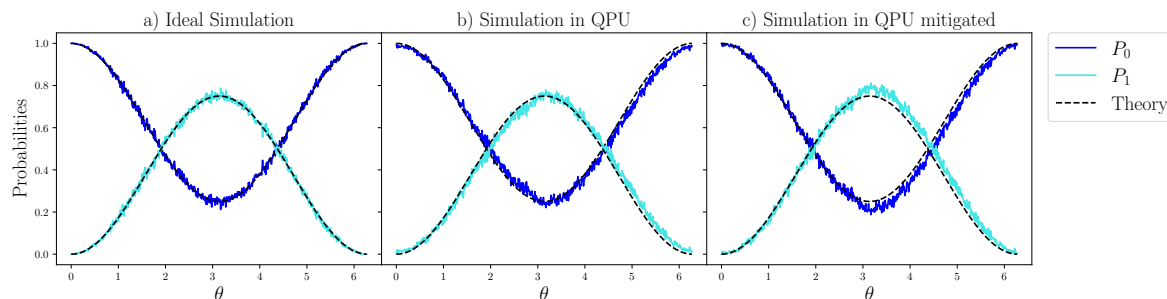


Figure 6. a) Ideal simulation of the circuit in figure 1 in the `qasm_simulator`, performed in a local (not quantum) simulator. b) Simulation in the `ibmq_lima` QPU exhibits some bias with respect to the theoretical result, indicating the presence of hardware errors that affect the measurement probabilities. c) Simulation using the `qiskit` measurement error mitigator does not significantly improve error.

The computer simulation, made with 1024 shots, displays some fluctuations around the theoretical results of P_0 and P_1 , given by equations (2) and (3). The results of a simulation in the `ibmq_lima` QPU are slightly separated from the theoretical curve, due to imperfect evolution (imperfect quantum gates, decoherence, dissipation) and measurement errors. Qiskit measurement error mitigator, which takes into account the errors due to the state preparation and measurement (SPAM), does not significantly improve the estimation. State estimation is biased because our model does not faithfully describe the QPUs. A better model would incorporate corrections to the expressions for the probabilities P_0 and P_1 . In this work, however, we do not construct an improved model because our main objective is to assess the performance of the estimator of s_z as a function of the parameter θ , and not of its implementation. Hence, we proceed as if our estimator were unbiased.

The simulations, performed in the `ibmq_lima` QPU for three different values of θ (see Table 1), qualitatively agree with the expected results, including the fact that the estimations with $\theta = \pi$ have lower variances.

The qTTF can also be experimentally measured, using a state 2-design, which is set of states X satisfying

$$\int d\psi \langle \psi | O_1 | \psi \rangle \langle \psi | O_2 | \psi \rangle = \frac{1}{|X|} \sum_{\psi \in X} \langle \psi | O_1 | \psi \rangle \langle \psi | O_2 | \psi \rangle, \quad (22)$$

for all operators O_1, O_2 [31]. Here, $|X|$ is the number of elements of X . It is easy to see that F^{-1} can be written as $\langle \psi | O_1 | \psi \rangle \langle \psi | O_2 | \psi \rangle$, where $O_1 = \frac{1}{2} (1 + \cos^2 \frac{\theta}{2}) + \frac{1}{2} \sin^2 \frac{\theta}{2} \sigma_z$

Table 1. Estimation (\hat{s}_z) of the z spin component for the six eigenstates of the Pauli matrices, in `qasm_simulator` classical simulator and the IBM `ibmq_lima` QPU, for the angles $\theta = \pi, 2\pi/3, \pi/2$. Each state was simulated five times with 5×1024 shots each.

Simulator	State	s_z	$\hat{s}_z (\theta = \pi)$	$\hat{s}_z (\theta = 2\pi/3)$	$\hat{s}_z (\theta = \pi/2)$
QASM	$ \psi_{z0}\rangle$	1.0	1.00 ± 0.00	1.00 ± 0.00	1.00 ± 0.00
	$ \psi_{z1}\rangle$	-1.0	-1.00 ± 0.00	-1.03 ± 0.02	-0.99 ± 0.06
	$ \psi_{x0}\rangle$	0.0	0.00 ± 0.04	-0.01 ± 0.04	-0.01 ± 0.05
	$ \psi_{x1}\rangle$	0.0	0.01 ± 0.02	0.00 ± 0.01	0.01 ± 0.06
	$ \psi_{y0}\rangle$	0.0	0.00 ± 0.02	-0.02 ± 0.04	0.03 ± 0.03
	$ \psi_{y1}\rangle$	0.0	0.01 ± 0.04	0.01 ± 0.03	0.01 ± 0.04
IBMQ	$ \psi_{z0}\rangle$	1.0	0.95 ± 0.06	0.96 ± 0.04	0.94 ± 0.06
	$ \psi_{z1}\rangle$	-1.0	-0.92 ± 0.08	-0.8 ± 0.2	-0.8 ± 0.2
	$ \psi_{x0}\rangle$	0.0	-0.04 ± 0.05	0.00 ± 0.01	0.03 ± 0.09
	$ \psi_{x1}\rangle$	0.0	0.1 ± 0.1	0.1 ± 0.1	0.2 ± 0.2
	$ \psi_{y0}\rangle$	0.0	0.00 ± 0.02	-0.03 ± 0.05	-0.01 ± 0.02
	$ \psi_{y1}\rangle$	0.0	0.06 ± 0.07	0.1 ± 0.1	0.1 ± 0.1

and $O_2 = \frac{1}{2} \csc^2 \frac{\theta}{2} (1 - \sigma_z)$. We use $X = \{|\psi_{z0}\rangle, |\psi_{z1}\rangle, |\psi_{x0}\rangle, |\psi_{x1}\rangle, |\psi_{y0}\rangle, |\psi_{y1}\rangle\} = \left\{ |0\rangle, |1\rangle, \frac{|0\rangle+|1\rangle}{\sqrt{2}}, \frac{|0\rangle-|1\rangle}{\sqrt{2}}, \frac{|0\rangle+i|1\rangle}{\sqrt{2}}, \frac{|0\rangle-i|1\rangle}{\sqrt{2}} \right\}$, that is, the set of eigenvectors of the three Pauli matrices.

From the simulation results, we can build N samples to make an estimation of s_z as it is described in Appendix A.1. In figure 7 we compare the average of variances of the estimations and the qTTF parameter over N for the six states of the three Pauli matrices. We can see how the Cramér-Rao bound is satisfied since $\overline{\text{Var}(\hat{s}_z)} \geq \overline{\text{qTTF}}/N$. As $N \rightarrow \infty$ we see that we are reaching the equality of the Cramér-Rao bound.

3.2. Complete qubit state estimation

For the complete qubit state estimation model, the interaction (11) with the optimal parameters was simulated using the `qasm_simulator` and the `ibmq_lima` QPU. We consider the six eigenstates of the three Pauli spin matrices, $\{|\psi_{z0}\rangle, |\psi_{z1}\rangle, |\psi_{x0}\rangle, |\psi_{x1}\rangle, |\psi_{y0}\rangle, |\psi_{y1}\rangle\}$. Each state was estimated by averaging the results of five estimations; each estimation used 1024 shots. The fidelity between the initial state of the system ρ_0^S and the estimated state $\hat{\rho}_0^S$, $\mathcal{F}(\rho_0^S, \hat{\rho}_0^S) = [\text{Tr} \sqrt{\sqrt{\rho_0^S} \hat{\rho}_0^S \sqrt{\rho_0^S}}]^2$, is low (reaching just 33% for $|\psi_0\rangle = |\psi_{x0}\rangle$), as shown in Table 2.

This error in the estimation of the total spin Bloch vector is a consequence of the number of gates needed to simulate this system (around 44 CNOT gates and 82 single-qubit gates). Another quantity that helps to understand the low fidelity of the estimated states is the circuit depth, the largest number of gates, from the input to the output, always moving ahead along qubit wires. The transpiled circuit that represents the evolution operator, has a circuit depth of 83.

Even if this is already a low probability for having a good simulation, we have not

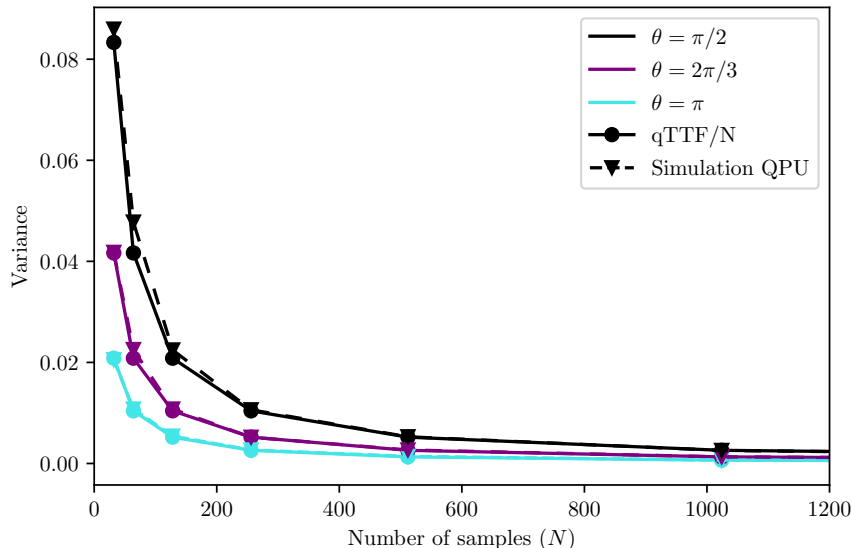


Figure 7. Graph of the qTTF parameter $\overline{F^{-1}}$ and variance of the estimations of N samples, for the angles $\theta = \pi, 2\pi/3, \pi/2$.

Table 2. Estimation $(\hat{s}_x, \hat{s}_y, \hat{s}_z)$ of the Bloch vector $\vec{s} = (s_x, s_y, s_z)$ corresponding to the eigenstates of the three Pauli operators, using the optimal values of the circuit parameters θ_A and θ_B approximately 3.45 and -8.42 respectively. Estimations were executed in `qasm_simulator` classical simulator and the IBM `ibmq_lima` QPU, using 5×1024 shots.

Simulator	State	s_x	\hat{s}_x	s_y	\hat{s}_y	s_z	\hat{s}_z	Fidelity
QASM	$ \psi_{z0}\rangle$	0.0	-0.01 ± 0.06	0.0	-0.03 ± 0.08	1.0	0.94 ± 0.04	99.7%
	$ \psi_{z1}\rangle$	0.0	-0.02 ± 0.07	0.0	-0.02 ± 0.03	-1.0	-0.97 ± 0.03	99.8%
	$ \psi_{x0}\rangle$	1.0	0.99 ± 0.02	0.0	-0.01 ± 0.04	0.0	-0.00 ± 0.06	99.8%
	$ \psi_{x1}\rangle$	-1.0	-0.992 ± 0.007	0.0	0.04 ± 0.01	0.0	0.02 ± 0.08	99.8%
	$ \psi_{y0}\rangle$	0.0	-0.01 ± 0.04	1.0	0.94 ± 0.06	0.0	0.05 ± 0.04	99.8%
	$ \psi_{y1}\rangle$	0.0	0.01 ± 0.08	-1.0	-0.994 ± 0.004	0.0	0.05 ± 0.06	99.7%
IBMQ	$ \psi_{z0}\rangle$	0.0	-0.60 ± 0.08	0.0	0.2 ± 0.1	1.0	0.75 ± 0.07	85%
	$ \psi_{z1}\rangle$	0.0	-0.7 ± 0.2	0.0	0.34 ± 0.07	-1.0	0.3 ± 0.3	37%
	$ \psi_{x0}\rangle$	1.0	-0.3 ± 0.3	0.0	0.2 ± 0.1	0.0	0.7 ± 0.2	32%
	$ \psi_{x1}\rangle$	-1.0	-0.75 ± 0.07	0.0	0.1 ± 0.1	0.0	0.5 ± 0.2	92%
	$ \psi_{y0}\rangle$	0.0	-0.75 ± 0.04	1.0	0.17 ± 0.08	0.0	0.63 ± 0.06	55%
	$ \psi_{y1}\rangle$	0.0	-0.5 ± 0.2	-1.0	0.2 ± 0.1	0.0	0.74 ± 0.08	41%

taken into account other error sources, such as state preparation and measurements errors (SPAM), as well as those related to coherence time [32, 33]; which justify even more the low fidelities obtained in Table 2.

In figure 8 we take N samples of spin estimations for each of the six eigenstates of the Pauli matrices and compare the mean of the qTTF parameter over N and the

average of the covariance matrix trace. The Cramér-Rao bound $\overline{\text{Cov}(s, s')} \geq \overline{q\text{TTF}}/N$ is not only always satisfied, but it also provides a good estimation for the variance.

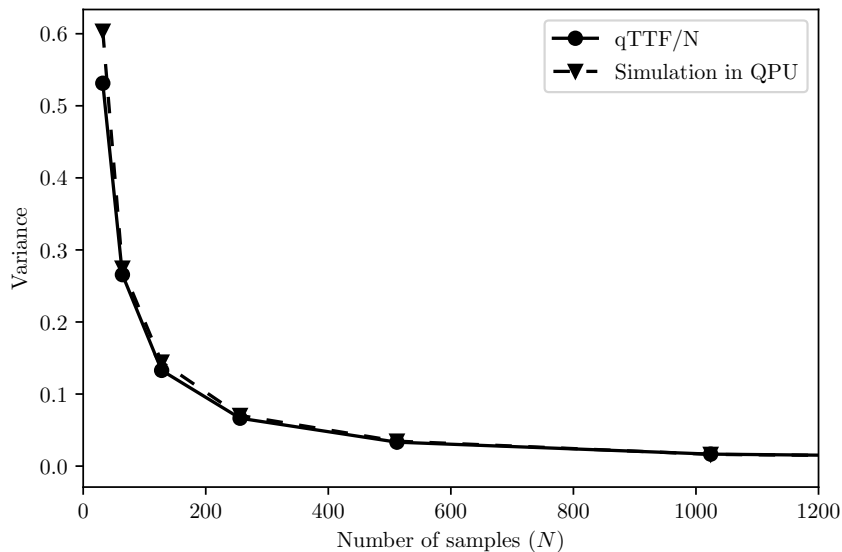


Figure 8. Mean of the qTTF error parameter over N and trace of the covariance matrix means over the six eigenstates of the Pauli matrix against the N samples.

3.3. Optimal complete qubit state estimation

Low fidelity results found before are not a characteristic of the tomographic method employed, but from the implementation in noisy quantum computers. We modify the U_{AB} operator in equation (12), minimizing the number of CNOTs gates used. The resulting circuit is shown in fig. 9.

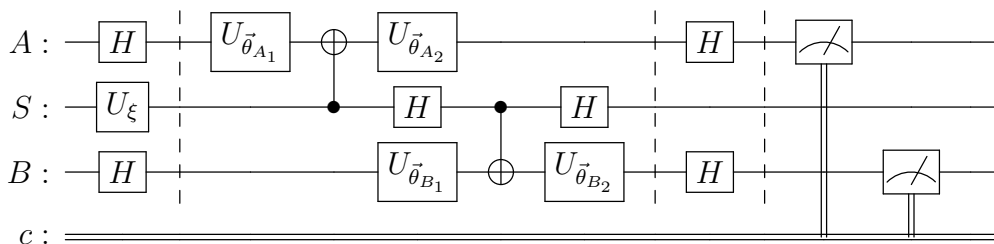


Figure 9. Quantum circuit proposed for optimal complete qubit state estimation in NISQ quantum computers.

The circuit in figure 9 depends on twelve parameters, three for each U gate, $U(\vec{\theta}) = U(\theta, \phi, \lambda) = \begin{pmatrix} \cos(\theta) & -e^{i\lambda} \sin(\theta) \\ e^{i\phi} \sin(\theta) & e^{i(\phi+\lambda)} \cos(\theta) \end{pmatrix}$. Optimization of qTTF over these parameters is made using random initial parameters. The best parameters

$$\begin{aligned} \vec{\theta}_{A_1} &= (0.59, 1.58, 2.52), & \vec{\theta}_{A_2} &= (2.55, 1.94, 0.31), \\ \vec{\theta}_{B_1} &= (0.70, 4.31, 3.46), & \vec{\theta}_{B_2} &= (0.67, 6.47, 4.47), \end{aligned}$$

correspond to an average error $\bar{\Delta} \approx 8$.

The estimation of the quantum state is good enough by linear inversion, which relies on linear regression estimation algorithms [34]. Thus, it has a lower computational cost with respect to the model in subsection 3.2 which performs tomography using a maximum likelihood estimation algorithm. The results of state estimation for the six eigenstates of the Pauli operators to perform the estimation protocol can be found in Table 3. The fidelities of the estimated states are above 98% when the model of figure 9 is implemented in an IBM QPU.

Table 3. Estimation ($\hat{s}_x, \hat{s}_y, \hat{s}_z$) of the Bloch vector $\vec{s} = (s_x, s_y, s_z)$ corresponding to the eigenstates of the three Pauli operators, using the optimal circuit described in figure 9. Estimations were executed in `qasm_simulator` classical simulator and the IBM `ibmq_lima` QPU, using 5×1024 shots.

Simulator	State	s_x	\hat{s}_x	s_y	\hat{s}_y	s_z	\hat{s}_z	Fidelity
QASM	$ \psi_{z0}\rangle$	0.0	0.00 ± 0.07	0.0	-0.02 ± 0.02	1.0	1.00 ± 0.06	99.8%
	$ \psi_{z1}\rangle$	0.0	0.01 ± 0.05	0.0	0.03 ± 0.05	-1.0	-0.99 ± 0.05	99.8%
	$ \psi_{x0}\rangle$	1.0	0.95 ± 0.04	0.0	0.02 ± 0.01	0.0	0.03 ± 0.01	99.9%
	$ \psi_{x1}\rangle$	-1.0	-1.00 ± 0.02	0.0	-0.02 ± 0.05	0.0	0.00 ± 0.05	99.9%
	$ \psi_{y0}\rangle$	0.0	-0.04 ± 0.03	1.0	1.02 ± 0.03	0.0	-0.05 ± 0.07	99.7%
	$ \psi_{y1}\rangle$	0.0	0.00 ± 0.05	-1.0	-1.01 ± 0.07	0.0	0.02 ± 0.05	99.9%
IBMQ	$ \psi_{z0}\rangle$	0.0	0.12 ± 0.04	0.0	0.05 ± 0.03	1.0	0.96 ± 0.03	99.5%
	$ \psi_{z1}\rangle$	0.0	-0.14 ± 0.03	0.0	0.01 ± 0.03	-1.0	-0.81 ± 0.04	99.2%
	$ \psi_{x0}\rangle$	1.0	0.93 ± 0.04	0.0	0.14 ± 0.03	0.0	0.04 ± 0.04	99.2%
	$ \psi_{x1}\rangle$	-1.0	-0.88 ± 0.04	0.0	-0.09 ± 0.04	0.0	0.15 ± 0.04	98.9%
	$ \psi_{y0}\rangle$	0.0	-0.00 ± 0.06	1.0	0.87 ± 0.03	0.0	0.14 ± 0.04	99.1%
	$ \psi_{y1}\rangle$	0.0	0.10 ± 0.05	-1.0	-0.75 ± 0.03	0.0	0.02 ± 0.09	99.1%

4. Conclusions

We reviewed qubit tomographic models that make use of one or two parameters, enabling the estimation of a single component or the entire Bloch vector associated with the initial state of the qubit, respectively. We use tomography techniques that rely on either linear regression estimators or the discrete maximum-likelihood estimator. These models are based on the interaction between the qubit under study and one or two auxiliary qubits that act as meters. We used the quantum tomographic transfer function (qTTF), the

trace of the inverse of the Fisher information matrix averaged over all pure states, as a measure of the global error of the models. The qTTF, which displays enormous variations as a function of the parameters of the models, is significantly higher for the models which aim to completely estimate the state. The best complete estimation model has a global error about 25 times larger than its single-component counterpart.

For the case of one component estimation, the smallest global error is obtained for the value of the parameter which maximizes the entangling power of the associated unitary transformation. This suggests that entanglement between the system and the meter might play a role in the quality of the estimation. The estimation error for complete state estimation model, before averaging over the possible initial states of the system, presents moderate fluctuations as a function of the initial state.

We implemented both estimation models on an IBM QPU. Experimental results for several values of the parameter of the single-component model agrees well with the theoretical results, with small deviations due to imperfect evolution and measurement errors. The experimental errors corresponding to the best complete state estimation model, due to the number of CNOT and single-qubit gates of the implementation, are so large that the fidelity between the estimated and the prepared initial state of the qubit can be as low as 30%.

The fidelities obtained with a modified model, taking into account the natural interactions of the QPU, were above 98%. Additionally, the corresponding qTTF is half the error for the original complete state estimation optimal model.

The methodology employed in this work can be applied to other estimation models (states in larger Hilbert spaces, different system-meter interactions, unitary or dissipative evolution), although the optimization becomes increasingly difficult as the number of parameters (state and evolution) increases. These modifications of the estimation model can be performed taking into account the characteristics of the QPU, for example, its basis gates or topology. This makes the model practical for being adapted to any quantum device or any other research purpose, such as simulations of experimental setups.

Our estimation method can be extended to n qubits employing a strategy similar to the one reported in [35], in which each qubit interacts with only one auxiliary qubit. In our case, two auxiliary qubits and two CNOTs are necessary for each qubit, exactly as shown in Figure 9. In other words, state estimation of n qubits, $2n$ auxiliary qubits and $2n$ CNOT gates are required. Notice that the total number of outcomes corresponding to the measurement of σ_z for each auxiliary qubit is 2^{2n} , exactly the number of parameters of a general unnormalized density matrix for n qubits. Notice that single-observable tomography for n qubits requires n auxiliary qubits and $3n$ CNOT gates. In effect, for each qubit an auxiliary qubit is required [35] as mentioned before. An optimal circuit for general two qubit interaction requires at most 3 CNOT gates and 15 elementary one-qubit gates [36]. In practice, the topology of the QPUs pose additional constraints, which might considerably increase the number of required CNOT gates.

As a final comment, we would like to highlight the need for a general theory

of resource management for state estimation, addressing how different resources can be optimally substituted for one another. For example, our results suggest that n^2 local measurements are equivalent to a single local observable, n auxiliary qubits, $15n$ elementary qubit gates and $3n$ CNOT gates.

5. Acknowledgements

This research received no specific grant from any funding agency.

6. Conflict of interest

The authors have no conflicts of interest to declare.

7. Data Availability

The data as well as the codes that support the findings of this study are available from the corresponding authors on reasonable request.

Appendix A. Equivalence between the variance of the estimator and the Fisher Error parameter.

Appendix A.1. Estimation of s_z

From the experiment, we have a set of observations $S = \{s_k\}_{k=1}^N$. Here s_k takes the values $s_0 = s_z(1, 0, \theta)$ with probability $P_0 = p$ and $s_1 = s_z(0, 1, \theta)$ with probability $P_1 = 1 - p$, where s_z is given by eq. (4), $s_z(P_0, P_1, \theta) = \csc^2\left(\frac{\theta}{2}\right) (P_0 - P_1 - \cos^2\left(\frac{\theta}{2}\right))$.

Each random variable s_k has a Bernoulli probability distribution, while the set S has a binomial probability distribution.

The mean \bar{s} and variance σ^2 of the observations are given by

$$\bar{s} = \frac{1}{N} \sum_{k=1}^N s_k = \frac{n_0}{N} s_0 + \frac{n_1}{N} s_1, \quad \text{and}$$

$$\sigma^2 = \frac{1}{N-1} \sum_{k=1}^N (s_k - \bar{s})^2 = \frac{n_0(s_0 - \bar{s})^2}{N-1} + \frac{n_1(s_1 - \bar{s})^2}{N-1},$$

where n_0 is the number of s_0 observations and n_1 is the number of s_1 observations.

The variance can be written as

$$\sigma^2 = \frac{N}{N-1} f_0 f_1 (s_0 - s_1)^2$$

where $f_0 = \frac{n_0}{N}$ and $f_1 = \frac{n_1}{N}$. When $N \rightarrow \infty$, $f_0 \rightarrow P_0 = p$ and $f_1 \rightarrow P_1 = 1 - p$. Therefore, $\bar{s} \rightarrow s_0 p + s_1 (1 - p)$ and $\sigma^2 \rightarrow p(1 - p)(s_0 - s_1)^2$, which are the theoretical values of the mean and the variance of a Bernoulli distribution respectively.

When \bar{s} is taken as a stochastic variable, its variance is

$$\sigma^2(\bar{s}) = \frac{1}{N^2} \sum_{k=1}^N \sigma = \frac{1}{N-1} f_0 f_1 (s_0 - s_1)^2 = \frac{1}{N-1} F^{-1},$$

where we have used $\text{Var}(\alpha X) = \alpha^2 \text{Var}(X)$ with α constant, and $\text{Var}(\sum_k s_k) = \sum_{k=1}^N \text{Var}(s_k) = N\sigma$. Here, F^{-1} is the inverse of the (scaled) Fisher parameter, given by eq. (6).

Appendix A.2. Total spin estimation

Similarly, as we have done for the estimation of s_z , here we have a set of observations $S^i = \{s_k^i\}_{k=1}^N$ for the i -th component of the spin. Those observations come from the measurement of the meters A and B . Then, we can define the mean value for each direction of the spin as

$$\bar{s}^i = \frac{1}{N} \sum_{k=1}^N s_k^i = \frac{n_{00}}{N} s_{00}^i + \frac{n_{01}}{N} s_{01}^i + \frac{n_{10}}{N} s_{10}^i + \frac{n_{11}}{N} s_{11}^i,$$

where $i = x, y, z$. Here we have to take into account that $s^i = s^i(n_{00}, n_{01}, n_{10}, n_{11})$. Then, $s_{00}^i = s^i(N, 0, 0, 0)$, $s_{01}^i = s^i(0, N, 0, 0)$, $s_{10}^i = s^i(0, 0, N, 0)$, and $s_{11}^i = s^i(0, 0, 0, N)$. For convenience, we change the notation $n_{00} \rightarrow n_1$, $n_{01} \rightarrow n_2$, $n_{10} \rightarrow n_3$ y $n_{11} \rightarrow n_4$. The variances of these random variables, in each direction, are

$$\text{Var}(s_k^i) = \sigma^{i2} = \frac{1}{N-1} \sum_{k=1}^N (s_k^i - \bar{s}^i)^2.$$

This can be written, taking into account the explicit form of the mean, as

$$\sigma^{i2} = \frac{N}{N-1} \left(\sum_{l=1}^4 f_l (s_l^i - \sum_{m=1}^4 s_m^i f_m)^2 \right).$$

Indices n, l correspond to the 4 possible results of the meter's measurements. Similarly to the previous case, we have $f_l = \frac{n_l}{N}$. When $N \rightarrow \infty$, we have

$$\sigma^{i2} \rightarrow \sum_{l=1}^4 p_l (s_l^i - \sum_{m=1}^4 p_m s_m^i)^2.$$

In this limit, the mean value of the estimation in the i -th direction can be written as

$$\bar{s}^i \rightarrow p_1 s_1^i + p_2 s_2^i + p_3 s_3^i + p_4 s_4^i.$$

This relation can be written in the matrix form $\bar{\vec{s}} = \mathbb{S} \vec{p}$, where

$$\bar{\vec{s}} = \begin{pmatrix} 1 \\ \bar{s}^x \\ \bar{s}^y \\ \bar{s}^z \end{pmatrix}, \quad \mathbb{S} = \begin{pmatrix} 1 & 1 & 1 & 1 \\ s_1^x & s_2^x & s_3^x & s_4^x \\ s_1^y & s_2^y & s_3^y & s_4^y \\ s_1^z & s_2^z & s_3^z & s_4^z \end{pmatrix}, \quad \vec{p} = \begin{pmatrix} p_1 \\ p_2 \\ p_3 \\ p_4 \end{pmatrix}.$$

Here we have to take into account that $\sum_{k=1}^4 p_k = 1$.

Equation (18), $\vec{s} = \mathbb{T}^{-1}\vec{p}$, allows us to build an estimator $\hat{\vec{s}}$,

$$\hat{\vec{s}} = \mathbb{T}^{-1}\mathbb{S}^{-1}\vec{s} = \mathbb{G}\vec{s}.$$

The i -th component of its variance $\text{Var}(\hat{s}^i) = \text{Var}(\mathbb{G}\vec{s})$ is

$$\begin{aligned} \text{Var}(\hat{s}^i) &= \text{Var}\left(\sum_{j=0}^4 G_{ij}\bar{s}_j\right) = \sum_{j=0}^4 G_{ij}^2 \text{Var}\left(\frac{1}{N}\sum_{k=1}^N s_k^j\right) \\ &= \sum_{j=0}^4 G_{ij}^2 \frac{1}{N^2} \sum_{k=1}^N \sigma^{j^2}. \end{aligned}$$

In terms of the experimental results we have

$$\text{Var}(\hat{s}^i) = \frac{1}{N} \sum_{j=0}^4 G_{ij}^2 \sigma^{j^2} = \frac{1}{N} \left(\sum_{j=0}^4 G_{ij}^2 \sum_{l=1}^4 p_l (s_l^j - \sum_{m=1}^4 p_m s_m^j)^2 \right),$$

where we have used $\text{Var}(\alpha X) = \alpha^2 \text{Var}(X)$ with α constant, and $\text{Var}(\sum_k s_k^i) = \sum_{k=1}^N \text{Var}(s_k^i) = N\sigma^i$. Here $i, j = 0, x, y, z$. i.e. they label the components of the spin vector. The component 0 satisfy the normalization $s^0 = 1$, then, it is clear that $\text{Var}(\hat{s}^0) = 0$. On the other hand, indices l, m correspond to the four possible results of the meter's measurements, 00, 01, 10 and 11.

It can be numerically shown that (see the supplementary material)

$$\sum_{j=0}^4 G_{ij}^2 \sum_{l=1}^4 p_l (s_l^j - \sum_{m=1}^4 p_m s_m^j)^2 = (\mathbb{F}^{-1})_{ii},$$

which corresponds to the Fisher error (21).

Appendix B. Explicit expressions for coefficients a_μ , b_μ , and c_μ

Setting $\theta_C = \sqrt{\theta_A^2 + \theta_B^2}$, we can write the coefficients a_μ , b_μ , and c_μ as follows.

$$\begin{aligned}
a_0 &= \frac{1}{8} \cos\left(\frac{\theta_A}{2}\right) \left[\cos\left(\frac{\theta_A}{2}\right) + \frac{\theta_B \sin\left(\frac{\theta_B}{2}\right) \sin\left(\frac{\theta_C}{2}\right)}{\theta_C} + \cos\left(\frac{\theta_B}{2}\right) \cos\left(\frac{\theta_C}{2}\right) \right], \\
a_1 &= \frac{1}{8} \sin\left(\frac{\theta_A}{2}\right) \left[\sin\left(\frac{\theta_B}{2}\right) \cos\left(\frac{\theta_C}{2}\right) - \frac{\theta_B \cos\left(\frac{\theta_B}{2}\right) \sin\left(\frac{\theta_C}{2}\right)}{\theta_C} \right], \\
a_2 &= -\frac{\theta_A \sin\left(\frac{\theta_A}{2}\right) \sin\left(\frac{\theta_B}{2}\right) \sin\left(\frac{\theta_C}{2}\right)}{8\theta_C}, \\
a_3 &= -\frac{1}{8} \sin\left(\frac{\theta_A}{2}\right) \left[\frac{\theta_A \cos\left(\frac{\theta_B}{2}\right) \sin\left(\frac{\theta_C}{2}\right)}{\theta_C} + \sin\left(\frac{\theta_A}{2}\right) \right], \\
c_0 &= \frac{1}{32} \left[4 \cos\left(\frac{\theta_C}{2}\right) \cos\left(\frac{\theta_A}{2} + \frac{\theta_B}{2}\right) + \cos(\theta_A - \theta_B) + \cos(\theta_A) + \cos(\theta_B) + 1 \right], \\
c_1 &= \frac{1}{8} \left[\cos\left(\frac{\theta_A}{2}\right) \sin\left(\frac{\theta_B}{2}\right) \sin\left(\frac{\theta_A - \theta_B}{2}\right) - \frac{\theta_B \sin\left(\frac{\theta_C}{2}\right) \sin\left(\frac{\theta_A + \theta_B}{2}\right)}{\theta_C} \right], \\
c_2 &= -\frac{1}{8} \sin\left(\frac{\theta_A}{2}\right) \sin\left(\frac{\theta_B}{2}\right) \sin\left(\frac{\theta_A - \theta_B}{2}\right).
\end{aligned}$$

The remaining coefficients can be written in terms of the previous ones as $b_0(\theta_A, \theta_B) = a_0(\theta_B, \theta_A)$, $b_1(\theta_A, \theta_B) = a_3(\theta_B, \theta_A)$, $b_2(\theta_A, \theta_B) = -a_2(\theta_B, \theta_A)$, $b_3(\theta_A, \theta_B) = a_1(\theta_B, \theta_A)$, $c_3(\theta_A, \theta_B) = c_1(\theta_B, \theta_A)$.

References

- [1] Feynman RP. Simulating physics with computers. *International Journal of Theoretical Physics*. 1982;21.
- [2] Feynman RP. Quantum mechanical computers. *Foundations of Physics*. 1986;16.
- [3] Shor PW. Algorithms for quantum computation: discrete logarithms and factoring. In: *Proceedings 35th Annual Symposium on Foundations of Computer Science*; 1994. p. 124-34.
- [4] Grover LK. A Fast Quantum Mechanical Algorithm for Database Search. In: *Proceedings of the Twenty-Eighth Annual ACM Symposium on Theory of Computing*. STOC '96. New York, NY, USA: Association for Computing Machinery; 1996. p. 212-9. Available from: <https://doi.org/10.1145/237814.237866>.
- [5] Kiktenko EO, Kublikova DN, Fedorov AK. Estimating the precision for quantum process tomography. *Optical Engineering*. 2020;59(6):1 9. Available from: <https://doi.org/10.1117/1.0E.59.6.061614>.
- [6] Gaikwad A, Shende K, Arvind, Dorai K. Implementing efficient selective quantum process tomography of superconducting quantum gates on IBM quantum experience. *Scientific Reports*. 2022 Mar;12(1):3688. Available from: <https://doi.org/10.1038/s41598-022-07721-3>.
- [7] Banaszek K, Cramer M, Gross D. Focus on quantum tomography. *New Journal of Physics*. 2013 dec;15(12):125020. Available from: <https://doi.org/10.1088/1367-2630/15/12/125020>.
- [8] James DFV, Kwiat PG, Munro WJ, White AG. Measurement of qubits. *Phys Rev A*. 2001 Oct;64:052312. Available from: <https://link.aps.org/doi/10.1103/PhysRevA.64.052312>.

- [9] Bechmann-Pasquinucci H, Tittel W. Quantum cryptography using larger alphabets. *Phys Rev A*. 2000 May;61:062308. Available from: <https://link.aps.org/doi/10.1103/PhysRevA.61.062308>.
- [10] Dong D, Petersen IR. Quantum estimation, control and learning: opportunities and challenges. *Annual Reviews in Control*. 2022.
- [11] Gupta R, Xia R, Levine RD, Kais S. Maximal Entropy Approach for Quantum State Tomography. *PRX Quantum*. 2021 Feb;2:010318. Available from: <https://link.aps.org/doi/10.1103/PRXQuantum.2.010318>.
- [12] Gupta R, Levine RD, Kais S. Convergence of a Reconstructed Density Matrix to a Pure State Using the Maximal Entropy Approach. *The Journal of Physical Chemistry A*. 2021;125(34):7588-95. PMID: 34410718. Available from: <https://doi.org/10.1021/acs.jpca.1c05884>.
- [13] Lohani S, Searles TA, Kirby BT, Glasser RT. On the Experimental Feasibility of Quantum State Reconstruction via Machine Learning. *IEEE Transactions on Quantum Engineering*. 2021;2:1-10.
- [14] Lukens JM, Law KJH, Jasra A, Lougovski P. A practical and efficient approach for Bayesian quantum state estimation. *New Journal of Physics*. 2020 Jun;22(6):063038. Available from: <https://dx.doi.org/10.1088/1367-2630/ab8efa>.
- [15] Qi B, Hou Z, Wang Y, Dong D, Zhong HS, Li L, et al. Adaptive quantum state tomography via linear regression estimation: Theory and two-qubit experiment. *npj Quantum Information*. 2017 Apr;3(1):19. Available from: <https://doi.org/10.1038/s41534-017-0016-4>.
- [16] Jamiołkowski A. Minimal number of operators for observability of N -level quantum systems. *International Journal of Theoretical Physics*. 1983;22(4):369-76.
- [17] Czerwiński A. Optimal evolution models for quantum tomography. *Journal of Physics A: Mathematical and Theoretical*. 2016;49(7):075301.
- [18] Czerwinski A. Selected Concepts of Quantum State Tomography. *Optics*. 2022;3(3):268-86.
- [19] D'Ariano GM. Universal quantum observables. *Physics Letters A*. 2002;300(1):1-6.
- [20] Peres A. When is a quantum measurement? *American Journal of Physics*. 1986;54(8):688-92. Available from: <https://doi.org/10.1119/1.14505>.
- [21] Saavedra D, Fonseca-Romero KM. Complete and incomplete state estimation via the simultaneous unsharp measurement of two incompatible qubit operators. *Phys Rev A*. 2019 Apr;99:042130. Available from: <https://link.aps.org/doi/10.1103/PhysRevA.99.042130>.
- [22] Řeháček J, Teo YS, Hradil Z. Determining which quantum measurement performs better for state estimation. *Phys Rev A*. 2015 Jul;92:012108. Available from: <https://link.aps.org/doi/10.1103/PhysRevA.92.012108>.
- [23] Pereira L, Zambrano L, Delgado A. Scalable estimation of pure multi-qubit states. *npj Quantum Information*. 2022 May;8(1):57. Available from: <https://doi.org/10.1038/s41534-022-00565-9>.
- [24] Kay SM. *Fundamentals of Statistical Signal Processing: Estimation Theory*. Prentice Hall PTR; 1993.
- [25] Benenti G, Casati G, Strini G. *Principles of Quantum Computation and Information*. vol. 2. World Scientific; 2004. Available from: <https://www.worldscientific.com/doi/abs/10.1142/5528>.
- [26] Zanardi P, Zalka C, Faoro L. Entangling power of quantum evolutions. *Phys Rev A*. 2000 Aug;62:030301. Available from: <https://link.aps.org/doi/10.1103/PhysRevA.62.030301>.
- [27] Paris M, Řeháček J. *Quantum State Estimation*. Springer, Berlin, Heidelberg; 2004. Available from: <https://link.springer.com/book/10.1007/b98673>.
- [28] Teo YS. *Introduction to Quantum-State Estimation*. World Scientific; 2015. Available from: <https://www.worldscientific.com/doi/abs/10.1142/9617>.
- [29] Řeháček J, Hradil Z, Knill E, Lvovsky AI. Diluted maximum-likelihood algorithm for quantum tomography. *Phys Rev A*. 2007 Apr;75:042108. Available from: <https://link.aps.org/doi/10.1103/PhysRevA.75.042108>.

- [30] Virtanen P, Gommers R, Oliphant TE, Haberland M, Reddy T, Cournapeau D, et al. SciPy 1.0: Fundamental Algorithms for Scientific Computing in Python. *Nature Methods*. 2020;17:261-72.
- [31] Bendersky A, Pastawski F, Paz JP. Selective and efficient quantum process tomography. *Phys Rev A*. 2009 Sep;80:032116. Available from: <https://link.aps.org/doi/10.1103/PhysRevA.80.032116>.
- [32] Jattana MS, Jin F, De Raedt H, Michielsen K. General error mitigation for quantum circuits. *Quantum Information Processing*. 2020 Nov;19(11):414. Available from: <https://doi.org/10.1007/s11128-020-02913-0>.
- [33] Unruh WG. Maintaining coherence in quantum computers. *Phys Rev A*. 1995 Feb;51:992-7. Available from: <https://link.aps.org/doi/10.1103/PhysRevA.51.992>.
- [34] Qi B, Hou Z, Li L, Dong D, Xiang G, Guo G. Quantum State Tomography via Linear Regression Estimation. *Scientific Reports*. 2013 Dec;3(1):3496. Available from: <https://doi.org/10.1038/srep03496>.
- [35] Wang H, Zheng W, Yu Y, Jiang M, Peng X, Du J. Determining an n-qubit state by a single apparatus through a pairwise interaction. *Physical Review A*. 2014;89(3):032103.
- [36] Vatan F, Williams C. Optimal quantum circuits for general two-qubit gates. *Physical Review A*. 2004;69(3):032315.